The Thimble
A Proactive Device for Water Main Maintenance

Authors
Achilles Batista, David McIntosh, Brock Taylor

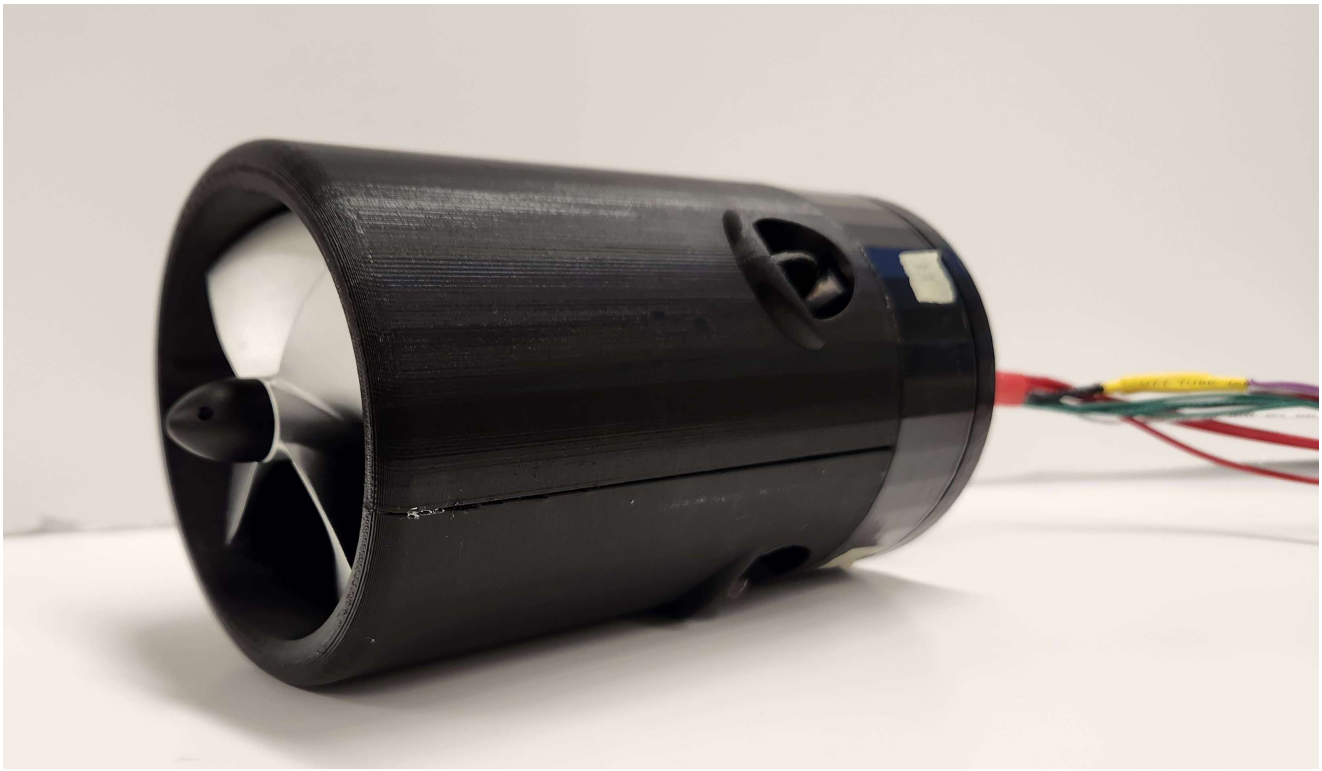

The authors are with the Department of Mechanical Engineering, Columbia University, New York, NY (mab2413@columbia.edu, dgm2158@columbia.edu, btt2115@columbia.edu. This material is based upon work developed in the MECE E3420 / E3430 Engineering Design Courses

***Abstract*— The Thimble is a tethered submersible device designed to explore water mains in search of leaks, cracks, and corrosion. After being inserted through the top valve of a fire hydrant, the Thimble navigates to the water main to collect data, which it sends to its operator through the tether. The Thimble is propelled by a central motor that directs flow to four angled output channels, allowing it to advance forward and change direction. The flow through these channels is controlled using a system of butterfly valves, which open and close to push the Thimble in the desired direction. The Thimble is revolutionary in the field of leak detection for collecting internal pipe data without the need to excavate water mains or shut off flow.**

I. Introduction

Civil infrastructure provides numerous services necessary to make living in densely packed cities possible, but none are more important than facilitating consistent access to clean water. As many cities around the world face water scarcity due to droughts, unsafe chemicals, and the overuse of natural resources, it is important that this resource is not taken for granted. However, an immense amount of water is lost every year, with a huge gulf between the amount of water supplied and what actually gets received. In New York City, 16-24% of all water is lost or otherwise unaccounted for by the end of its journey from upstate reservoirs, contributing to over 200 million gallons lost per day [1] [2]. These losses come from numerous sources - leaks, wastage, and metering miscalculations all contribute to this massive quantity of unaccounted for water. Each of these sources of water loss should ideally be mitigated, but to do so would be outside of the scope of a singular senior design project. Thus, it was decided to focus specifically on addressing leaks as a source of loss. Even this represents a very large problem space - leaks can occur in the tunnels and aqueducts that deliver water from reservoirs to the city, in the water mains that distribute it beneath the street level, and within the pipes of individual homes and businesses. These range from over 21 feet in diameter to less than an inch, and so problems that address issues in one set of pipes can be completely inapplicable for others [3]. Considering this, the topic was specified further to focus exclusively on water main leaks.

In New York, these underground pipes are the jurisdiction of the Department of Environment Protection (the DEP), and in an ideal world they would be replaced and maintained on a regular schedule. However, the DEP replaces less than 1% of the city's pipes each year, due to which over 40% of the city's water mains are over 80 years old [4] [5]. This slow rate of turnover allows failing water mains to be overlooked for decades before finally breaking, with these ancient pipes contributing a large portion of the city's 400 yearly water main bursts [5]. While there are many methods for detecting pipe leaks within homes, only a few are designed to analyze these water mains. Most of these devices utilize acoustic sensing techniques that listen for the sound of subterranean leaks, but this is not a preventative measure and can only work once a break has already occurred. There are a few devices designed to search for cracks prior to the pipe bursting, but these all require either the flow of water to be cut off or the pipe to be dug up and 'trenched', both of which are time consuming and unpopular with the general public. A method for detecting water main cracks prior to a leak beginning, and doing so without requiring the loss of any public services, would be a major boon for the city's leak prevention capabilities.

To address this opening, we have designed the Thimble, a rendering of which is shown in Fig. 1. The Thimble is a tethered submersible device which can be used by DEP operators to search pipes for cracks non-invasively, without needing to excavate the pipe in order to reach it. This is possible because the Thimble can enter the water main network through any fire hydrant, making the water main network accessible from street level. The Thimble has three main components - the spool, the tether, and the submersible. The spool attaches directly to the hydrant used for water main access, and unfurls to allow the Thimble's tether to extend. The tether is a steel-reinforced cable that ensures the Thimble cannot become detached from the spool and can be retracted at any time. The tether also houses cables that allow power and signals to run to and from the spool to the Thimble, preventing any need for an on-board battery and allowing a live data feed from the submersible. The submersible (often itself referred to as the Thimble) is cylindrical in shape and houses a central propeller to advance itself forward through the water main network, four butterfly valves to provide turning control, and both an inertial measurement unit (IMU) and a camera for collecting data. These electronics are housed inside a watertight chamber, which has been sealed using a combination of epoxy, sealing screws, gaskets, o-rings, and cable glands. All materials used in the thimble's construction are FDA approved to not contaminate the city's water supply, and the waterproofing methods are heavily tested in order to ensure no short circuits will occur for the internal electronics.

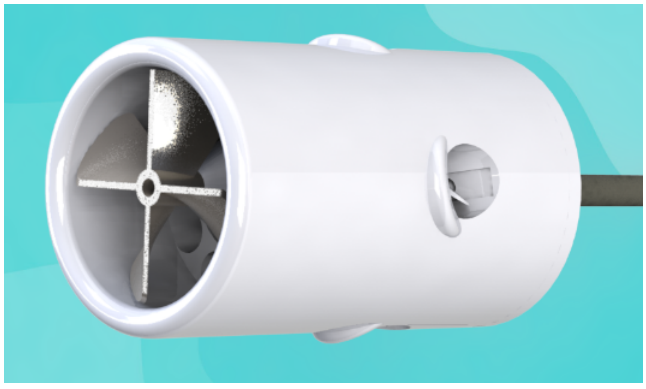

Fig. 1. 3D rendering of the Thimble's submersible

The Thimble is intended for use by DEP professionals, who will first cut off water from the water main to the fire hydrant closest to the mains they intend to survey. Critically, this does not involve cutting off the water in the main itself, only the water going to the hydrant. Then, they would unscrew the top cap of the hydrant, remove the hydrant's branch valve, and in place of the cap attach the Thimble's

spool. This spool would be made of bronze or cast iron, the same materials as the rest of the hydrant it is attached to, and will be secured by screwing it into place using the same 1.5" NH / NST (National Hose / National Standard Thread) used on traditional hydrants [6]. Water will then be allowed to flow back into the hydrant, and once any internal turbulence has died down, the submersible will begin to unspool its tether and drop into the water main network (route shown in Fig. 2). While the pipes themselves range from 6 to 18 inches in diameter, the Thimble must first pass through the hydrant's main valve - an opening only 4.5-5.25 inches in diameter, depending on the hydrant [6]. For this reason, the submersible has been designed with a maximum outer diameter of 4.3 inches to fit through all gaps it will encounter.

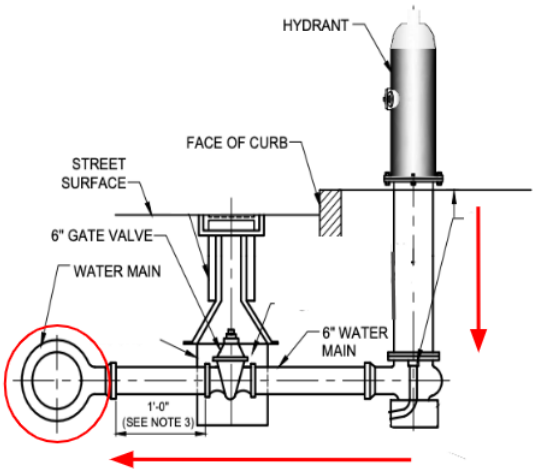

Fig. 2. Map of the Thimble's route from hydrant to water main [6]

The submersible itself has been 3D printed using PLA, which is coated in epoxy to render it watertight. In order to minimize 3D printing time and allow for rapid design iterations, its body is divided into three components - an upper left, upper right, and bottom section. The upper left and upper right pieces of the Thimble's body come together to hold its central motor, an APISQUEEN Brushless Waterproof 4650, which propels the Thimble forward [7]. In order to gain control over how the Thimble moves and turns, the flow from this propeller is diverted through four side channels which eject water at a 45 degree angle, as shown in Fig. 3. Each of these channels features a butterfly valve, which can open and close to either block flow or allow water to pass through unhindered. By closing three valves and leaving one open, this ensures that all flow will exit through the singular open valve, pushing the Thimble in the opposite direction. The 45 degree tilt of these channels ensures that each gives side-to-side position control as well as ejecting enough of the flow backwards to also propel the Thimble forwards. Backwards motion capabilities are unnecessary, because the tether can always be respooled to retract the Thimble and retrace its steps. One concern of this design is that the spin of the Thimble's single motor could cause the entire submersible to twirl, twisting its tether and making the camera feed difficult to analyze. To counteract this, each outflow channel is offset from the Thimble's central axis by a small distance, in order to induce an opposite torque and neutralize the propeller's spin.

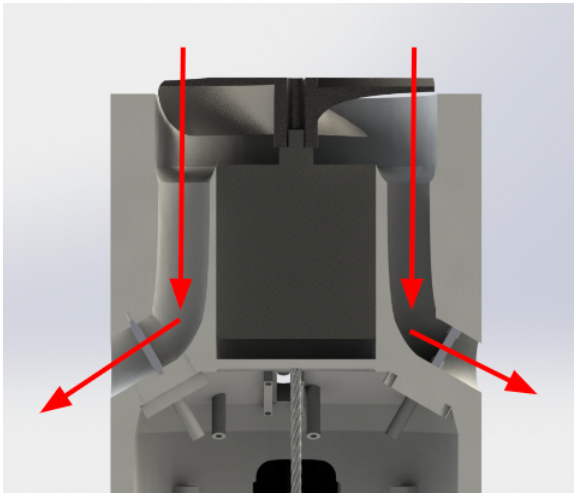

Fig. 3. Cross sectional view of the Thimble. Flow generated by the propeller exits each channel at a 45 degree angle

The Thimble's back chamber is the most thoroughly waterproofed segment, as it houses a number of fragile electronic components. This is where the camera, IMU, and all four servos are housed. Each servo motor is screwed into a custom-cut gasket to ensure a watertight seal, doubly protected by an o-ring on the shaft of each butterfly valve. The IMU and camera are both attached to the back cap of the chamber, which allows the camera to see outside of the Thimble through an acrylic window (illuminated by an accompanying LED). Both ends of this chamber feature a cable gland, which allows wiring to enter and exit the waterproof area, and two internal hooks present an attachment point for the tether's internal steel cable. This results in no loads being applied to the Thimble's wiring, and all strain diverted to the high strength cable.

II. Analysis 1: Wall Thickness FEA

A. Methods

One relevant concern in the Thimble's design is its ability to withstand the ambient pressures of operating within the city's water mains. While submerged, the Thimble will experience up to a pressure of 60 psi on all sides, contrasted with the 15 psi air pressure in NYC [8]. As the watertight electronics chamber will be sealed prior to the Thimble entering the water, there will be a 45 psi pressure differential between the exterior and interior chambers of the Thimble. It is critical that the Thimble be able to withstand this pressure difference without deforming, as this could lead to a gasket seal leaking and the watertight electronics chamber flooding. In order to determine if the Thimble's walls would hold without deforming, a finite element analysis in Solidworks was conducted.

For this analysis, a 45 psi pressure was applied to all exterior faces, as is shown in Fig. 12 in Appendix A. In this analysis, all exterior components of the Thimble were

modeled as a single piece, and all interior components were neglected. This means that the servos, valves, and wiring are non-existent in this model, and there are no gaps between the left, right, and bottom sections of the Thimble. To ensure that the results of this study are physically representative, a mesh convergence was also conducted. This found a difference of only 6.5% across successive meshes, which is low enough to proceed, but not beneath the 5% threshold for complete confidence (see Fig. 14 in Appendix A). As such, a factor of safety of 5 or higher (compared to the typical value of 3 used for most ductile materials) was sought after in order to assuage concerns about irregularities in the simulation.

B. Results

The von Mises stress concentration, shown in Fig. 4, gives a range of $3.320*10^2$ to $7.958*10^6 N/m^2$. The displacement plot, shown in Fig. 5, gives a maximum displacement of 0.2589 mm. These result in a factor of safety of 5.617 at the points of highest stress concentration.

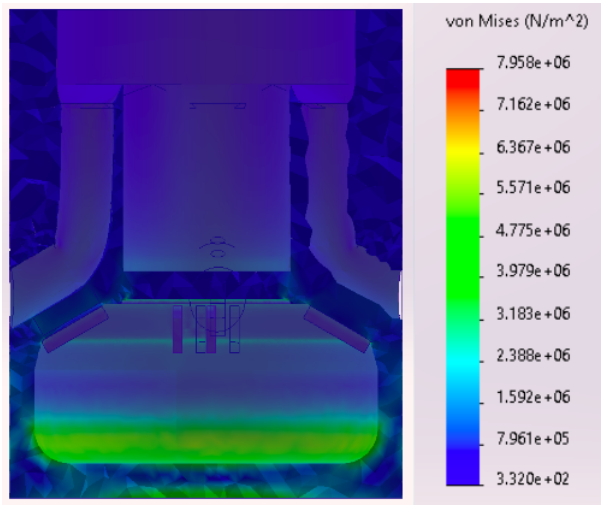

Fig. 4. FEA of von Mises Stress due to 45 PSI

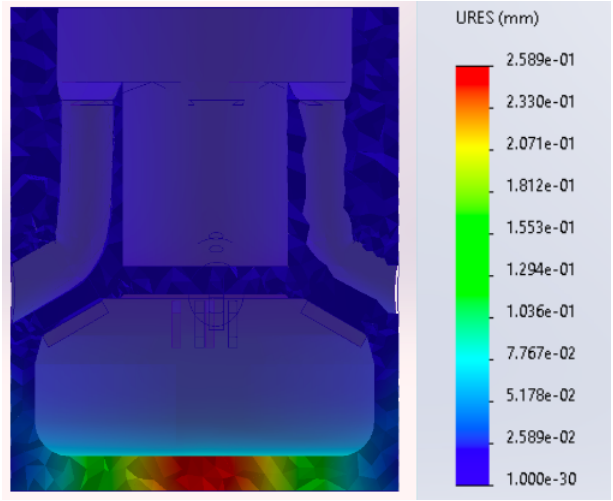

Fig. 5. FEA of displacement due to 45 PSI

C. Discussion

The stress concentrations resulting from these pressures are highest around the lip of the Thimble's back face, as well as at the center of Thimble's back cap. Similarly, the highest displacement was also observed at the center of the back cap. These results are logical, as the back cap appears as a wide and unsupported plane, able to be buckled inwards by a sufficiently large pressure. The main concern would be displacement large enough to affect waterproofing mechanisms. However, a displacement of 0.2589 mm is small enough to not risk disruption at this or any other location on the Thimble's body. It is orders of magnitude smaller than the Thimble's wall thickness, and with a factor of safety of over 5.6, it can safely be assumed that the current wall thicknesses are sufficient to hold the Thimble's body intact.

As multiple assumptions have been made when simplifying this CAD model, there are many sources of potential error. The mesh convergence did not reach a stable value less than 5%, potentially indicating the presence of an undetected corner and infinite stress concentration point, which would drastically skew the results toward higher stresses. Additionally, while a quarter of a millimeter is an extremely small distance, this has been compared against the wall thickness of the Thimble rather than the thickness of a gasket. On this frame of reference it is a much more notable displacement, and the resulting factor of safety for this would be substantially lower. This is not a glaring omission, as all gaskets are screwed into place with no room to be displaced into, but the effects of high pressures on them are still worth considering.

Additionally, this FEA is not without its shortcomings and omissions. Foremost among these is the removal of any seams and gaps in the Thimble's model, as in practice there are a number of attachment points between the upper and lower components of the Thimble. Each of these points is accompanied by a gasket, and so could become a failure point if they were to undergo a large deformation - but as the Thimble is treated as monolithic in this study, they are not covered by this FEA. This is a source of overconfidence in these results, and could be addressed by dividing this single FEA into multiple smaller pressure analyses on individual parts of the Thimble.

III. Analysis 2: Cable Attachment FEA

Given the risks associated with putting anything in a municipality's water supply, various critical failures had to be designed for. The worst case scenario in the operation of the Thimble is a failure in the physical connection from the tether and subsequently losing the device in the pipe, with no way to tell where it is. The Thimble could possibly travel for a long time in the water main, damaging the pipe as it moves, until it likely blocks flow at a junction, requiring dewatering of the pipe and trenching to remove the Thimble from the main. To prevent such a catastrophic failure, it is critical that the Thimble be secured at all times. To this end, one component of the tether's design is a steel cable which would attach to the thimble's main body and secure

it. The weakest point of this design is where it attaches to the Thimble, since the attachment point has to be strong enough to withstand the force from the cable. The Thimble would have two of the cable attachments illustrated below.

A. Methods

Finite element analysis was performed on the cable attachment to determine the forces it needed to withstand for proper functioning. The forces and constraints were modeled with the bolt holes being fixed in place and the curved slots experiencing a force upwards, representing the force that the cable applies. This can be seen in Fig. 15 and Fig. 16. The force for the cable was determined by looking at the manufacturer's table for the thrust of the motor, seen in Fig. 17 at 24 volts and 10 amps, which was 4.54 kg [7]. Then this thrust value was converted to a force by multiplying by the gravitational constant, 9.81 m/s^2, and dividing it by two, since the load would be shared between two identical attachment parts.

B. Results

With the conditions set, the FEA returned figures illustrating the stress and factor of safety of the part, seen in Fig.6 and Fig.7, respectively. Additionally, the von Mises stress was checked at different mesh sizes to verify that the mesh converged and it is shown in Fig.18 that the difference between the last two points is about 3%, which is well within the acceptable range.

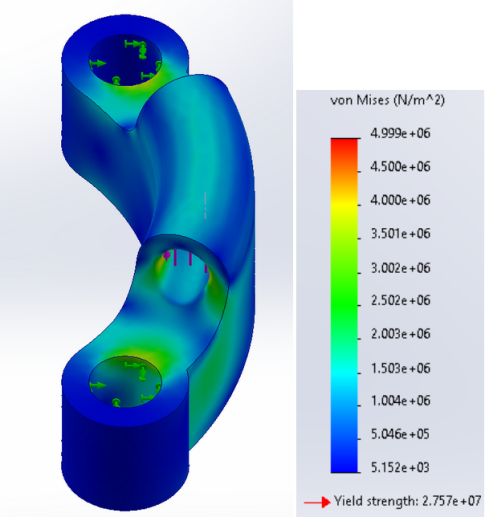

Fig. 6. Results of the FEA showing the von Mises stress throughout the part

C. Discussion

Once the analysis was completed, a minimum factor of safety of 5.5 was attained, which is within the desired range for the part. The data shown is the final result of various iterations of analyses which informed some change in the design of the attachment part. It was originally designed to be made from plastic to match the rest of the body, but due to the size constraints of the part and the initial FEA

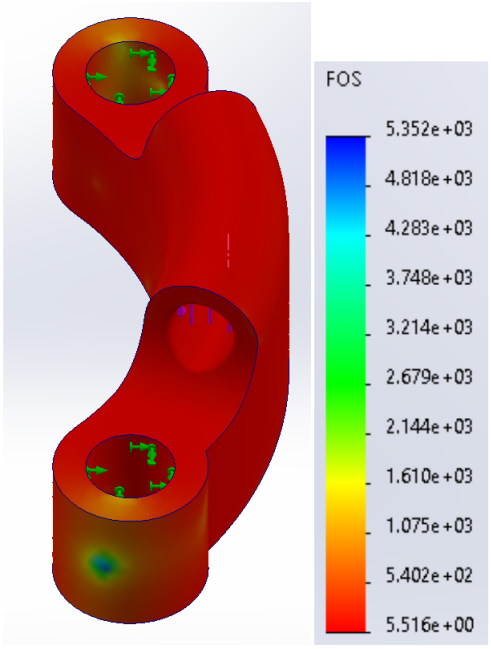

Fig. 7. Results of the FEA showing the factor of safety throughout the part

giving back a very low factor of safety, the high strength to weight ratio of aluminum made it a more suitable choice of material. Additionally, this analysis prompted the reshaping and resizing of the part to make it larger, for the sake of strength, and simpler, to minimize stress concentrations in the part. A possible source of error in this analysis is that it was assumed the steel cable would act evenly on the top of the inside face of the curved slot, but it will likely apply a force to the sides of the channel at some angle. Additionally, since steel cable does not bend very well, there could be stress concentrations at the corners of the curved slot, where the cable comes out. This was mitigated to some extent by the curvature of the channel, though not entirely because the channel does not curve upwards, only to the side. A future iteration of the analysis would try different curved angles for the slots to see how the factor of safety of the part could be maximized. Additionally, computational fluid dynamics analysis (CFD) would be performed on the geometry of the Thimble to determine what drag forces it would experience in the pipe and use those results to ensure that the part can also withstand extreme conditions due to drag.

IV. Analysis 3: Motor Analysis

In order for the Thimble to be able to navigate through pipes successfully, a sufficient understanding of its control characteristics is crucial. The goal of this analysis was to produce a torque-speed curve for the Thimble. Since a method for measuring torque was unavailable, current was measured instead since current and torque for DC motors are related by a constant. This test was run at a constant voltage by varying the Pulse Width Modulation (PWM) signal sent to the Electronic Speed Controller (ESC). Since the test was run under water, it is not the actual torque-motor curve but rather the intersection of this curve with the load curve of the water. Using this information, a plot of the electrical power

vs rotational velocity of the propeller was created. This information could be used in the future to better understand the control system dictating the thimble in order to create a robust controller.

A. Methods

The full assembly of the thimble was placed underwater. A power supply was used to supply a constant voltage of 8V to the ESC as well as measure the maximum current draw seen during use. The Thimble was held stationary and ran at a specified PWM output signal for 7 seconds. After waiting for approximately 3 seconds for it to get to steady state, a slow-motion video was taken of the propeller. A mark on the propeller was used in reference to a mark on the fish tank to determine rotations. This visual tachometer method allowed for the determination of rotational speed by counting the number of frames needed for a quarter of a rotation. While counting for a full rotation would be more accurate and less prone to disturbances, a quarter rotation was chosen for two reasons. First, some of the slower speeds did not reach a full rotation in the duration of one slow-motion video. Second, since frames were counted manually, counting a quarter rotation was faster. The frame rate of the camera used for the slow-motion video was 960 frames per seconds. By dividing the number of frames needed to reach a quarter of a rotation by this frame rate, the real time taken for the quarter rotation was determined. From this, the rotational speed in radians per second was calculated. The conversion from frame count to rotational velocity in units of rad/s is captured in Eq. 1 where N is the number of frames needed to reach a quarter of a rotation.

$$\omega = \frac{\pi/4}{(N/960)} \tag{1}$$

7 different PWM signals were used as input ranging from 77 to 95. PWM signals convert to duty cycle of the output signal by Eq. 2. A PWM input of 75 yields no output to the motor, 50 results in full throttle in reverse, and 100 results in full throttle forward. Anything in between can be roughly approximated as an effective voltage for the motor by multiplying the duty cycle by the input voltage. For example, a duty cycle of 77 on an input voltage of 8 would result in an effective voltage of 0.32V. For each of the PWM signal values tested, 5 trials were taken. For each trial, the maximum current reached during the trial was recorded as well as the steady state rotational velocity.

$$D = 100(\frac{x - 75}{50})\% \tag{2}$$

B. Results

Fig. 8 shows data collected from 7 different PWM signal values, for each of which 5 trials were taken. A logarithmic regression trendline is shown with an R^2 value of 0.96

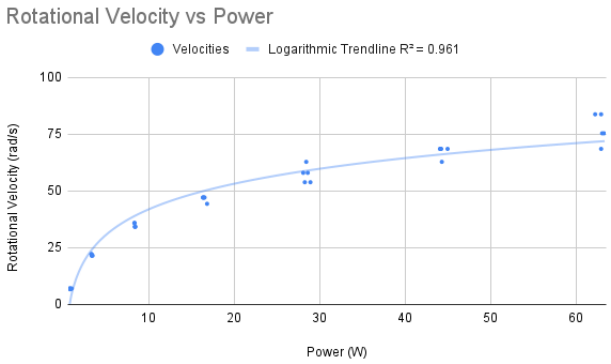

Fig. 8. Scatter plot of all data collected and trendline

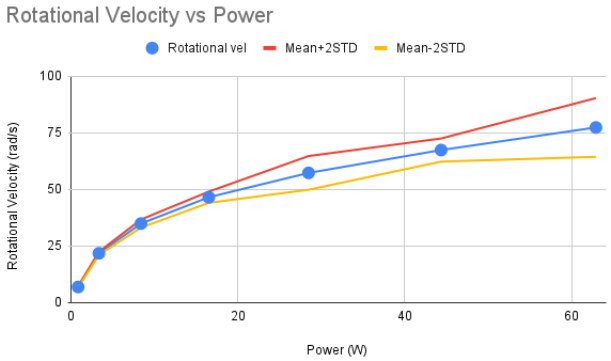

Fig. 9. Plot of rotational velocities vs power with 2σ error bars

Fig. 9 displays the average rotational velocity plotted against the average power at each PWM input signal. Additionally, error bars representing +/- 2 standard deviations of rotational velocity for each data point are displayed. This gives a 99% confidence interval of rotational velocity for each power value.

C. Discussion

Fig. 19 in Appendix A shows the average power vs the average rotational velocity at each PWM input signal. Error bars representing +/- 2 standard deviations of power for each data point are displayed, giving a 99% confidence interval of power for each rotational velocity value. Very little variance was observed in the current measurements as evident in this plot. However, non-negligible variation was observed in the rotational velocity as evident in Fig. 9. The variance of the rotational velocity also increased at higher speeds. This is likely a sensor issue due to the methodology in which these measurements were taken. Rotational velocities were determined based on the number of frames it took for the propeller to make a quarter rotation. At low velocities, this amounted to around 100 frames. However, at higher velocities, this was around 10-12 frames. Because of this, a difference of 1 frame lead to significantly higher variability at higher speeds than lower speeds. It also became harder at higher speeds to determine the exact number of frames needed for a quarter rotation, as the amount the propeller moves between frames is higher. This means it is more likely for a quarter rotation to lie between two frames, and

a somewhat arbitrary decision would need to be made on which frame to count. Because of these factors, the variance in rotational velocities became increasingly significant as the rotational velocity itself increased.

This effect could have been reduced by counting the number of frames for a full rotation or even for two full rotations during these faster tests. However, a quarter rotation was kept in order to maintain consistency with the slower tests in which a full rotation could not be counted. Another way to organize this test would be to set up more markers and count the amount the propeller rotated in a given number of frames. However, this would still have variability due to difficulty in obtaining this measurement objectively. Additionally, the measurements of rotational velocity and current were assumed to be independent - that is the potential covariance between these data was ignored. Based on the plots, this seems to have been a reasonable assumption, as little to no covariance in these data appears to be prevalent.

One potential issue that was a concern during testing was aliasing when measuring the rotational velocities. In order to ensure this was not a factor, measurements were started at a very low rotational speed and slowly increased over the trials. No abrupt changes in the data were observed to indicate that aliasing had occurred. Additionally, the fastest frequency observed was around 14 rotations per second which is far below the camera frame rate of 960 frames per second. Even considering the maximum quarter rotation rate of 56 Hz, this is still far below the camera frame rate. Because of these factors, it was confidently determined that aliasing had not occurred during data collection.

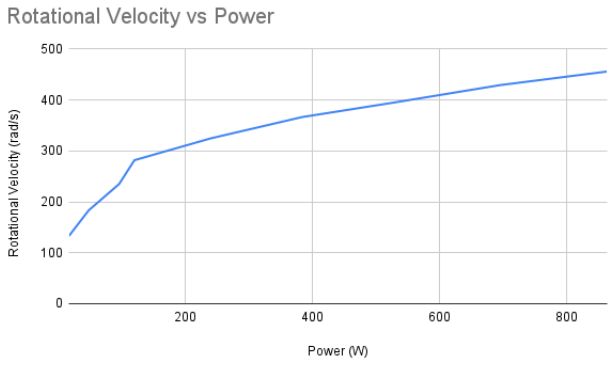

Fig. 10. Plot of rotational velocities vs power based on manufacturer specifications

Shown in Fig. 10 are APISQUEEN's specifications for the rotational velocity vs power plot given an input voltage of 24V. This information was taken from Fig. 17 in Appendix A [7]. Based on the general shape being the same, the validity of the testing done on the Thimble to produce the same plot is supported.

In testing the Thimble with this setup, a power supply with a current maximum of 10A was used. In order to ensure the Thimble did not surpass this limit during testing, a relatively low input voltage of 8V was supplied. However, this input voltage is significantly different from the 24V testing data provided by APISQUEEN, and therefore makes comparison difficult. Nevertheless, based on the PWM signal, it is possible to correlate data points despite the difference in input voltage. PWM signals command the ESC to output a specific duty cycle signal. Based on the duty cycle, an effective voltage can be determined as the average voltage of that output. With this method, despite the motor being tested by APISQUEEN at 24V and the Thimble being tested at 8V, some of the data points have the same effective voltage. However, this is not the case for all of the data due to the extreme difference in input voltage.

In order to get a sense of the efficiency loss due to the extra resistance placed on the motor by the Thimble, one data point can be correlated. The last data point on the Thimble was run at 8V with a duty cycle of 90%, giving an effective voltage of 7.2V. In Fig. 17, the motor being run at 24 volts and a duty cycle of 30% also gives an effective voltage of 7.2V. In APISQUEEN's testing, this resulted in an output current of 2A and an output speed of 1750 RPM. In testing the Thimble, an output current of 7.9A and an output speed of 740 RPM was found. This is a change of 395% in current draw and 42% in rotational speed. This indicates that the Thimble housing adds significant resistance to the motor, which was expected as it severely limits the cross sectional area through which water can flow.

Next steps in this testing set up would be to incorporate a load cell or some other method of measuring force. With this, a plot corresponding power to thrust or rotational speed to thrust could be created. Furthermore, additional tests being conducted at different input voltages could prove useful as a way of determining the exact relationships between power, rotational velocity, and voltage in order to develop a robust control system for the Thimble.

V. Conclusion

The thimble is a proactive leak detection device designed to enter water mains through fire hydrants, where it will provide position data and live video feed. Finite element analysis was conducted to fine tune the design of various components, such as the thickness of the walls of the Thimble and the attachment point to the tether. The wall thickness analysis supported the decision to make the back wall .375 inches, which provided a satisfactory factor and minimal displacement of the wall. Analysis of the attachment point determined that the part was best made thicker than initially designed and that it be made from aluminum. The largest electronic component on the Thimble, the propeller motor, was tested by applying a range of duty cycles to the motor through PWM input signals, to read the current draw and resulting rotational velocity. The data collected provides the foundational data required to develop a control algorithm for the Thimble, since its geometry would greatly affect the flow rate the propeller could send. The current prototype of the Thimble still requires development but demonstrates the feasibility of a water jet propelled submersible to navigate water mains and send back video to assess the condition of the pipe.

References

[1] A. Forman, C. for an Urban Future, F. Attard, T. Conrad, R. Ellison, E. Laskodi, H. Schultz, J. Silva, X. Wang, N. Zonis, A. Dowla, R. C. Markets, A. for a Better New York, B. F., A. B. G. Foundation, and F. for the City of New York, "Overdue investments for New York's aging infrastructure," tech. rep., 3 2014.

[2] "History of Drought Water Consumption - DEP."

[3] "600 feet below the Hudson River: Final concrete lining completed for $1billionwatertunnel,''$ 32021.

[4] J. Barron, "Water Mains Are Bursting All Over New York. Can They Be Fixed?," 2 2020.

[5] ASCE, "New York Infrastructure — ASCE's 2021 Infrastructure Report Card," 4 2024.

[6] "WATER MAIN STANDARD DRAWINGS," tech. rep., 12 2020.

[7] "ApisQueen brushless waterproof motor 4650 24V 960W for underwater thruster boat rov."

[8] D. Greeley, "Leak Survey DSGvs2Final," 11 2017.

VI. Appendix A

A. Analysis 1: Wall Thickness FEA

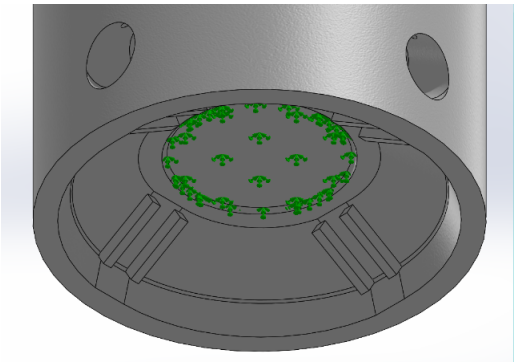

Fig. 11. Illustration of the fixtures used for the the wall thickness FEA

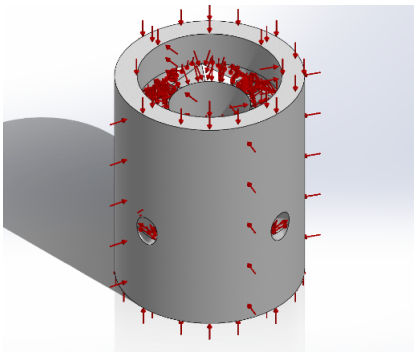

Fig. 12. External forces used for the the wall thickness FEA

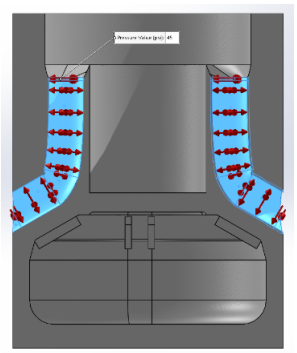

Fig. 13. Internal forces used for the the wall thickness FEA

B. Analysis 2: Cable Attachment FEA

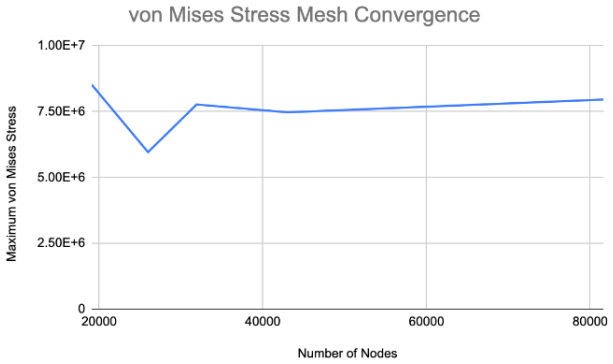

Fig. 14. Plot of Maximum von Mises Stress vs number of nodes for the Thimble under 45 PSI

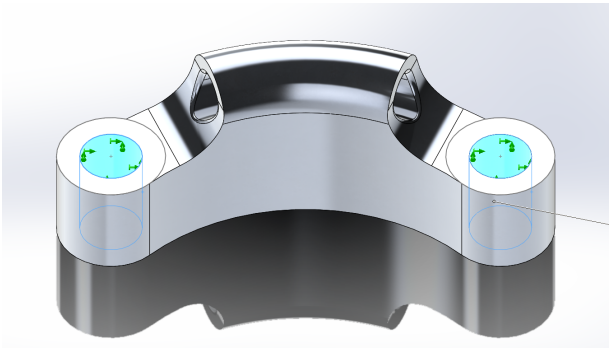

Fig. 15. Illustration of the fixtures used for the bolt holes in FEA

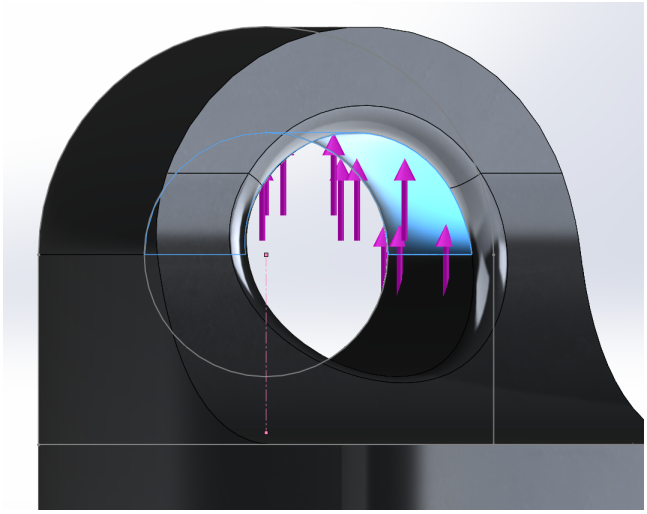

Fig. 16. Illustration of the force applied to the inside of the attachment part

C. Analysis 3: Motor Analysis

Forward					Reversal				
Voltage (V)	Throttle	Current (A)	RPM	Thrust (Kg)	Voltage (V)	Throttle	Current (A)	RPM	Thrust (Kg)
24	1.600ms	0.7	1268	0.73	24	1.400ms	0.8	1268	0.73
24	1.650ms	2	1750	1.36	24	1.350ms	2	1800	1.36
24	1.700ms	4	2245	2.36	24	1.300ms	4	2280	2.18
24	1.750ms	5	2691	3.63	24	1.250ms	5	2700	3.18
24	1.800ms	10	3100	4.54	24	1.200ms	11	3200	4.36
24	1.850ms	16	3500	6.17	24	1.150ms	16	3500	4.99
24	1.900ms	22	3771	7.53	24	1.100ms	21	3890	6.26
24	1.950ms	29	4100	8.80	24	1.050ms	27	4100	7.62
24	2.000ms	36	4354	9.98	24	1.000ms	34	4400	8.62

Fig. 17. Data table provided by APISQUEEN; the distributor of the underwater motor that was purchased for the project. [7]

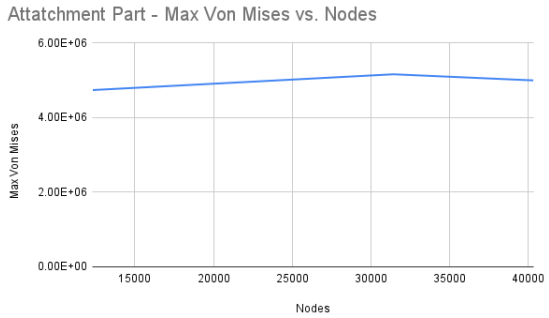

Fig. 18. Plot of Maximum von Mises Stress vs number of nodes in the model for the part which attaches to the tether to determine if the model converged

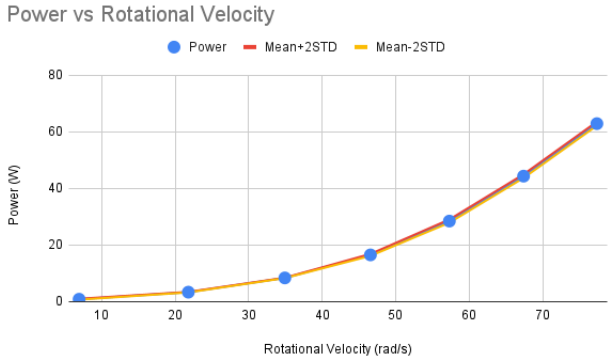

Fig. 19. Plot of power vs rotational velocities with 2σ error bars